Composite Structures 94 (2012) 2764–2776

Contents lists available at SciVerse ScienceDirect

Composite Structures

journal homepage: www.elsevier.com/locate/compstruct

Three-dimensional vibration analyses of functionally graded material rectangular plates with through internal cracks

C.S. Huang *, P.J. Yang, M.J. Chang

Department of Civil Engineering, National Chiao Tung University, 1001 Ta-Hsueh Rd., Hsinchu 30050, Taiwan

ARTICLE INFO

Article history:
Available online 11 April 2012

Keywords:
Three-dimensional elasticity theory
Ritz method
Functionally graded material
Cracked plate
Vibration

ABSTRACT

The free vibrations of rectangular FGM plates with through internal cracks are investigated using the Ritz method. Three-dimensional elasticity theory is employed, and new sets of admissible functions for the displacement fields are proposed to enhance the effectiveness of the Ritz method in modeling the behaviors of cracked plates. The proposed admissible functions accurately describe the stress singularities at the fronts of the crack and display displacement discontinuities across the crack. The correctness and validity of the present approach are established through comprehensive convergence studies and comparisons with published results for homogeneous cracked plates, based on various plate theories. The locally effective material properties of FGM in the thickness direction are estimated by a simple power law. The effects of the volume fraction of the constituents of FGM and the thickness-to-length ratio on the frequencies are investigated. Frequency data for FGM square plates with three types of boundary conditions along the four side faces and with internal cracks of various crack lengths, positions and orientations are tabulated for the first time.

1. Introduction

Laminated composite materials have been successfully utilized in engineering systems, particularly in aircraft and aerospace structures, primarily because they have excellent strength-to-weight and stiffness-to-weight ratios. Nevertheless, the abrupt change in material properties across the interface between material layers can produce large interlaminar stresses and cause delaminations. Recently, functionally graded materials (FGMs), which are heterogeneous composite materials and whose material properties vary continuously with a change in the volume fraction of its constituents, have been invented to overcome the disadvantages of conventional laminated composite materials. These have found various applications in various engineering fields. Functionally graded materials can be designed to have high resistance to temperature gradients, significant reduction in residual and thermal stresses, and high wear resistance.

Rectangular plates are very common structure components in real applications. Cracks in structural components cause local changes in the stiffness of the structure and may result in the changes to the global dynamic characteristics. If a cracked plate is in resonance, the crack can propagate very rapidly. To prevent fracture by such vibration, the vibration characteristics of the cracked plate must firstly be classified.

Most studies of the vibrations of cracked plates involve homogeneous plates and utilize different solution techniques and plate theories. Based on the classical plate theory, integral equation techniques [1–6], finite element methods [7,8], extended finite element method [9], and the Ritz method [10–13] have been applied to solve for the vibrations of cracked rectangular plates. Similarly, based on the first-order shear deformation plate theory, finite element solutions [14] and solutions obtained using the Ritz method [15,16] have also been proposed.

The research on vibrations of homogenous rectangular plates is extensive, but a number of studies of FGM rectangular plates, based on various plate theories, have also been published. Abrate [17] and Zhang and Zhou [18] demonstrated that an FGM thin plate behaves like a homogeneous plate if a proper reference plane is adopted in the classical thin plate theory. Based on the first-order shear deformation plate theory, Hosseini-Hashemi et al. [19] presented analytical solutions for the vibrations of a rectangular plate that was simply supported at its two opposite edges and was lying on either Winkler or Pasternak elastic foundations, and Zhao et al. [20] analyzed vibrations of square and skew plates under different combinations of boundary conditions using the element-free kp-Ritz method. Ferreira et al. [21] determined the vibration frequencies of square plates employing the first-order, third-order shear deformation plate theories and the collocation method with multiquadric radial basis functions. Using higher-order shear deformation plate theory, Qian et al. [22] applied the Petrov–Galerkin meshless method to find the vibration frequencies of FGM thick

* Corresponding author. Tel.: +886 3 5712121x54962; fax: +886 3 5716257.
E-mail address: cshuang@mail.nctu.edu.tw (C.S. Huang).

0263-8223/$ - see front matter © 2012 Elsevier Ltd. All rights reserved.
http://dx.doi.org/10.1016/j.compstruct.2012.04.003

simply-supported square plates, while Roque et al. [23] adopted the multiquadric radial basis function method to determine the vibration frequencies of FGM thick plates with various combinations of boundary conditions. Matsunaga [24] employed a 2D higher-order approximate plate theory and found analytical solutions for the vibrations of FGM simply-supported rectangular plates. Based on three-dimensional elasticity theory, Vel and Batra [25] presented exact solutions for the vibrations of simply supported plates, while Reddy and Cheng [26] provided an asymptotic solution using a transfer matrix approach. Uymaz and Aydogdu [27] showed numerical solutions for three-dimensional vibrations of plates with various combinations of boundary conditions using the Ritz method.

Only one published paper addresses the vibrations of cracked FGM plates. Huang et al. [28] utilized the Ritz method and Reddy's plate theory to study the vibrations of FGM thick plates with side cracks. No investigation of vibrations of FGM plates with internal cracks based on various plate theories or three-dimensional elasticity theory has been published. The main purpose of this study is to present accurate three-dimensional solutions for vibrations of rectangular FGM plates with through internal cracks that have arbitrary orientations and positions. Since the configurations under consideration are rather simple, the well-known Ritz method is adopted and the admissible functions include crack functions that are proposed properly to account for stress singularities at the fronts of an internal crack and to allow for displacement discontinuities across a crack. To ensure the admissible functions form a complete set, orthogonal polynomials are also included in the admissible functions.

The proposed solution is verified by comprehensive convergence studies and by comparisons with published solutions for homogeneous cracked plates that were obtained using various plate theories and methods. The accuracy of the present solution is further confirmed by comparisons with a finite element solution for an FGM cracked plate. Numerous non-dimensional frequencies and nodal patterns are reported herein for the first time for cracked rectangular FGM plates with various thickness-to-length ratios, different combinations of boundary conditions, and having internal cracks of various crack lengths, positions, and angles of inclination.

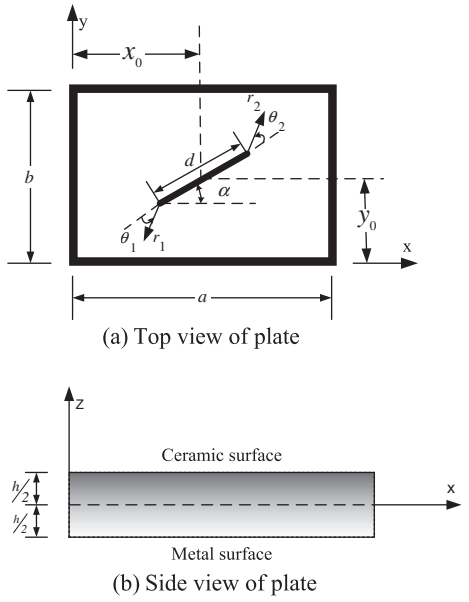

Fig. 1. A rectangular functionally graded material plate with an internal crack (x_0 and y_0 locate the center of the crack).

The effects of the volume fraction in the modeling of material distribution in the thickness direction on the vibration frequencies are also examined. The relevant results are presented in tables and figures as references for future research.

2. Geometric configuration and model of material properties

Fig. 1 displays a rectangular FGM plate (of length a, width b and thickness h) with an internal crack and also shows the rectangular coordinate (x, y, z) originating at the mid-plane of the plate. Two polar coordinates (r_1, θ_1) and (r_2, θ_2) originating at the two intersections of crack fronts with the mid-plane of the plate, respectively, are also given to describe the stress singularities as r_1 and r_2 approach zero. The configuration of the internal crack is defined by the mid-point of the crack in the mid-plane of the plate (x_0, y_0), the angle of inclination α, and the length of the crack, d.

The functionally graded material of interest is a mixture of metal and ceramics. The material properties (elastic modulus, $E = E(z)$, Poisson's ratio, $\upsilon = \upsilon(z)$, and mass density, $\rho = \rho(z)$) vary throughout the thickness of the plate in a manner determined by the volume fractions of the constituents. A power-law describes the variation of material properties in z direction:

$$P(z) = (P_t - P_b)V(z) + P_b, \tag{1a}$$

$$V(z) = \left(\frac{z}{h} + \frac{1}{2}\right)^{\bar{m}}, \tag{1b}$$

where P denotes a property of the material; P_t and P_b represent the properties at the top ($z = h/2$) and the bottom ($z = -h/2$) faces, respectively, and $\bar{m}$ is the parameter of volume fraction that governs the material variation profile in the thickness direction. The FGM plates considered herein are made of aluminum (Al) and ceramic (alumina (Al_2O_3)), whose material properties are given in Table 1 [24].

3. Methodology

The Ritz method is employed to determine the natural frequencies of an FGM plate with an internal crack because it has a very robust mathematical basis and is a very popular method for finding the natural frequencies of plates with simple geometry. In the Ritz method, the dynamic characteristics of the plate are predicted by minimizing the energy functional

$$\Pi = V_{\max} - T_{\max}, \tag{2}$$

where $V_{\max}$ and $T_{\max}$ are the maximum strain energy and the maximum kinetic energy of the plate under simple harmonic motion, respectively. According to three-dimensional elasticity theory,

$$V_{\max} = \frac{1}{2}\int_V \Big\{\lambda(z)(U_{1,x}+U_{2,y}+U_{3,z})^2 + G(z)[2(U_{1,x})^2 + 2(U_{2,y})^2 + 2(U_{3,z})^2 + (U_{1,y}+U_{2,x})^2 + (U_{2,z}+U_{3,y})^2 + (U_{3,x}+U_{1,z})^2]\Big\} dV \tag{3a}$$

$$T_{\max} = \frac{\omega^2}{2}\int_V \rho(z)\left(U_1^2 + U_2^2 + U_3^2\right) dV \tag{3b}$$

Table 1
Material properties of the FGM components.

Material	Properties		
	E (GPa)	Poisson's ratio (υ)	ρ (kg/m^3)
Aluminum (Al)	70	0.3	2702
Alumina (Al_2O_3)	380	0.3	3800

where

$$\lambda(z) = \frac{\upsilon(z)E(z)}{(1+\upsilon(z))(1-2\upsilon(z))}; \tag{4a}$$

$$G(z) = \frac{E(z)}{[2(1+\upsilon(z)]}; \tag{4b}$$

ω is the circular frequency of vibration; $U_i(x, y, z)$ $(i = 1, 2, 3)$ are the vibration amplitudes in x, y and z directions, respectively, and the subscript comma denotes partial differentiation with respect to the coordinate defined by the variable after the comma.

The Ritz method provides accurate solutions, whose accuracy and efficiency depend mainly on the proper choice on admissible functions. To obtain accurate solutions for vibrations of a plate with an internal crack, two sets of admissible functions are applied to approximate each of the mechanical displacement amplitude functions, $U_i(x, y, z)$. The mechanical displacement amplitude functions are expressed as

$$U_i = \widehat{U}_{ip} + \widehat{U}_{ic} \tag{5}$$

where $\widehat{U}_{ip}$ are expressed in terms of a set of polynomial functions, which form a mathematically complete set if an infinite number of terms are used; $\widehat{U}_{ic}$ are expressed in terms of a set of special functions to supplement the polynomials to describe appropriately the essential singular stresses at the crack fronts and displacement discontinuities across the crack.

A Gram–Schmidt process, proposed by Bhat [29], is utilized to construct orthogonal polynomials in the x and y directions, denoted by $P_j^{(i)}(x)$ and $Q_k^{(i)}(y)$, respectively. $\widehat{U}_{ip}$ is expressed as

$$\widehat{U}_{ip}(x,y,z) = f_i(z)\sum_{l=1}^{N_{iz}}\sum_{j=1}^{N_{ix}}\sum_{k=1}^{N_{iy}} A_{jkl}^{(i)} P_j^{(i)}(x) Q_k^{(i)}(y) z^{l-1} \quad (i = 1,2,3), \tag{6}$$

Notably, $P_j^{(i)}(x)$ satisfy the geometric boundary conditions for U_i on the faces of the plate, $x = 0$ and $x = a$, while $Q_k^{(i)}(y)$ satisfy the geometric boundary conditions for U_i on the faces, $y = 0$ and $y = b$. In Eq. (6), ordinary polynomials are used in the z direction to resemble the kinematic assumption of displacements that is made in the various shear deformation plate theories. Function $f_i(z)$ is selected to satisfy the geometric boundary conditions for U_i on the top and bottom faces. Herein, completely stress-free top and bottom surfaces are considered, such that $f_i(z) = 1$.

The functions in Eq. (6) are continuous everywhere and do not result in any stress singularities. Clearly, these functions do not improve the Ritz method by capturing a crack in the plate. In Eq. (3), the integration domain for an intact plate does not differ from that for a cracked plate. Consequently, if only the admissible functions in Eq. (6) are employed, then the effect of the crack on the behaviors of the plate cannot be reflected and the resulting solutions apply to an intact plate.

To make the Ritz method capable of taking into account the influence of a crack on the vibrations of the plate, some special functions are needed to describe accurately the behaviors of the plate along the crack. The two important features of the behaviors of the plate along the crack are stress singularities at the fronts of the internal crack and displacement discontinuities across the crack. Using three-dimensional elasticity theory, Hartranft and Sih [30] and Chaudhuri and Xie [31] showed that the order of the stress singularity at a crack front is -0.5 for a cracked homogenous plate with free–free crack-side boundary conditions. Huang and Chang [32,33] found that a cracked FGM plate has the same order of stress singularity as a homogenous plate.

Considering a homogenous wedge without loading and using the cylindrical coordinates shown in Fig. 2, Hartranft and Sih [30] proposed a series solution for displacement components with the following form

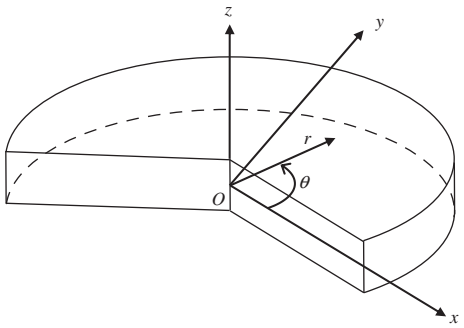

Fig. 2. Coordinates for a wedge.

$$u = \sum_{m=0}^{\infty}\sum_{n=0}^{\infty} r^{\lambda_m+n} U_n^{(m)}(\theta, z; \lambda_m),$$
$$\upsilon = \sum_{m=0}^{\infty}\sum_{n=0}^{\infty} r^{\lambda_m+n} V_n^{(m)}(\theta, z; \lambda_m), \quad w = \sum_{m=0}^{\infty}\sum_{n=0}^{\infty} r^{\lambda_m+n} W_n^{(m)}(\theta, z; \lambda_m) \tag{7}$$

where u, υ and w are the displacement components in r, θ and z directions, respectively. They found that

$$U_0^{(m)} = B_1^{(m)}(z)\cos(\lambda_m+1)\theta + B_2^{(m)}(z)\sin(\lambda_m+1)\theta + C_1^{(m)}(z) \times \cos(\lambda_m-1)\theta + C_2^{(m)}(z)\sin(\lambda_m-1)\theta \tag{8a}$$

$$V_0^{(m)} = -B_1^{(m)}(z)\sin(\lambda_m+1)\theta + B_2^{(m)}(z)\cos(\lambda_m+1)\theta + \frac{\lambda_m+3-4\upsilon}{\lambda_m-3+4\upsilon}\left[C_2^{(m)}(z)\cos(\lambda_m-1)\theta - C_1^{(m)}(z)\sin(\lambda_m-1)\theta\right] \tag{8b}$$

$$W_0^{(m)} = A_1^{(m)}(z)\cos\lambda_m\theta + A_2^{(m)}(z)\sin\lambda_m\theta \tag{8c}$$

When a crack with free crack surfaces is under consideration, $\lambda_m = m/2,\ m = 1, 2, 3, \ldots$ Wang [34] proposed the following set of functions included in the admissible functions of the Ritz solutions to describe the behaviors of a crack in vibrations of a rectangular plate with a side crack,

$$\left\{ z^k r^{(2n-1)/2}\cos\frac{2l+1}{2}\theta \ \text{ and } \ z^k r^{(2n-1)/2}\sin\frac{2l+1}{2}\theta \right| k=0,1,2,\ldots;\ l=0,1,2,\ldots,n;\ \text{and}\ n=1,2,3,\ldots \Big\}. \tag{9}$$

The solution terms corresponding to $n = 0$ and $\lambda_m = m/2$ with $m = 1, 3, 5, \ldots$ in Eq. (7) can be linearly expanded by the above set of functions.

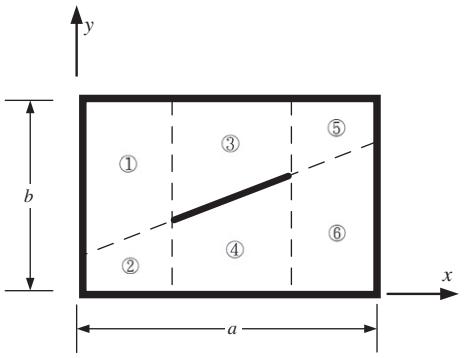

Fig. 3. Six sub-domains for integration in x–y plane.

Table 2
Convergence of frequency parameters $\omega(b^2/h)\sqrt{\rho/E}$ for a homogeneous SSSS square thin plate ($h/b = 0.05$) having a horizontal central crack with $d/a = 0.3$.

Mode No.	Crack functions (N_c)	Polynomial solution size ($N_x \times N_y$) at [ ] $N_z = 3$; ( ) $N_z = 4$; { } $N_z = 5$							Stahl and Keer [2]* and Huang et al. [16]+
		3×3	4×4	5×5	6×6	7×7	8×8	9×9	
1	0	[6.319]	[5.928]	[5.928]	[5.928]	[5.928]	[5.928]	[5.928]	5.70*, 5.589+
		(6.313)	(5.922)	(5.922)	(5.922)	(5.922)	(5.922)	(5.922)	
		{6.313}	{5.922}	{5.922}	{5.922}	{5.922}	{5.922}	{5.922}	
	2	[5.814]	[5.769]	[5.753]	[5.747]	[5.740]	[5.738]	[5.732]	
		(5.806)	(5.761)	(5.745)	(5.738)	(5.732)	(5.730)	(5.723)	
		{5.806}	{5.761}	{5.745}	{5.738}	{5.731}	{5.730}	{5.723}	
	4	[5.624]	[5.619]	[5.613]	[5.612]	[5.609]	[5.608]	[5.606]	
		(5.615)	(5.610)	(5.604)	(5.603)	(5.600)	(5.599)	(5.598)	
		{5.615}	{5.610}	{5.604}	{5.603}	{5.600}	{5.599}	{5.598}	
	5	[5.612]	[5.609]	[5.605]	[5.604]	[5.602]	[5.602]	[5.601]	
		(5.604)	(5.600)	(5.596)	(5.595)	(5.593)	(5.593)	(5.592)	
		{5.604}	{5.600}	{5.596}	{5.595}	{5.593}	{5.593}	{5.592}	
	6	[5.609]	[5.605]	[5.601]	[5.601]	[5.599]	[5.599]	[5.599]	
		(5.600)	(5.596)	(5.592)	(5.592)	(5.591)	(5.591)	(5.590)	
		{5.600}	{5.596}	{5.592}	{5.592}	{5.591}	{5.591}	{5.590}	
2	0	[17.82]	[17.51]	[14.69]	[14.69]	[14.65]	[14.65]	[14.65]	14.67*, 14.19+
		(17.77)	(17.45)	(14.66)	(14.66)	(14.62)	(14.62)	(14.62)	
		{17.77}	{17.45}	{14.66}	{14.66}	{14.62}	{14.62}	{14.62}	
	2	[15.45]	[15.10]	[14.38]	[14.34]	[14.31]	[14.29]	[14.29]	
		(15.41)	(15.06)	(14.34)	(14.30)	(14.27)	(14.26)	(14.25)	
		{15.41}	{15.06}	{14.34}	{14.30}	{14.27}	{14.26}	{14.25}	
	4	[14.30]	[14.28]	[14.28]	[14.27]	[14.26]	[14.26]	[14.26]	
		(14.26)	(14.24)	(14.24)	(14.23)	(14.22)	(14.22)	(14.22)	
		{14.26}	{14.24}	{14.24}	{14.23}	{14.22}	{14.22}	{14.21}	
	5	[14.28]	[14.27]	[14.27]	[14.26]	[14.26]	[14.25]	[14.25]	
		(14.24)	(14.23)	(14.22)	(14.22)	(14.22)	(14.21)	(14.21)	
		{14.24}	{14.23}	{14.22}	{14.22}	{14.22}	{14.21}	{14.21}	
	6	[14.26]	[14.26]	[14.26]	[14.25]	[14.25]	[14.25]	[14.25]	
		(14.22)	(14.22)	(14.22)	(14.21)	(14.21)	(14.21)	(14.21)	
		{14.22}	{14.22}	{14.22}	{14.21}	{14.21}	{14.21}	{14.21}	
3	0	[17.82]	[17.51]	[14.69]	[14.69]	[14.65]	[14.65]	[14.65]	14.90*, 14.55+
		(17.77)	(17.45)	(14.66)	(14.66)	(14.62)	(14.62)	(14.62)	
		{17.77}	{17.45}	{14.66}	{14.66}	{14.62}	{14.62}	{14.62}	
	2	[15.96]	[15.73]	[14.66]	[14.65]	[14.62]	[14.62]	[14.62]	
		(15.92)	(15.69)	(14.63)	(14.62)	(14.59)	(14.59)	(14.59)	
		{15.92}	{15.69}	{14.63}	{14.62}	{14.59}	{14.59}	{14.59}	
	4	[14.65]	[14.61]	[14.61]	[14.61]	[14.61]	[14.61]	[14.61]	
		(14.62)	(14.58)	(14.58)	(14.58)	(14.58)	(14.58)	(14.58)	
		{14.62}	{14.58}	{14.58}	{14.58}	{14.58}	{14.58}	{14.58}	
	5	[14.65]	[14.61]	[14.60]	[14.60]	[14.60]	[14.60]	[14.60]	
		(14.62)	(14.58)	(14.57)	(14.57)	(14.57)	(14.57)	(14.57)	
		{14.62}	{14.58}	{14.57}	{14.57}	{14.57}	{14.57}	{14.57}	
	6	[14.65]	[14.60]	[14.60]	[14.60]	[14.60]	[14.60]	[14.60]	
		(14.62)	(14.57)	(14.57)	(14.57)	(14.57)	(14.57)	(14.57)	
		{14.62}	{14.57}	{14.57}	{14.57}	{14.57}	{14.57}	{14.57}	
4	0	[27.49]	[27.13]	[23.24]	[23.24]	[23.18]	[23.18]	[23.18]	23.87*, 22.90+
		(27.37)	(27.01)	(23.17)	(23.17)	(23.11)	(23.11)	(23.11)	
		{27.37}	{27.01}	{23.17}	{23.17}	{23.11}	{23.11}	{23.11}	
	2	[25.08]	[24.20]	[23.13]	[23.11]	[23.07]	[23.06]	[23.06]	
		(24.98)	(24.11)	(23.05)	(23.03)	(22.99)	(22.98)	(22.98)	
		{24.98}	{24.11}	{23.05}	{23.03}	{22.99}	{22.98}	{22.98}	
	4	[23.09]	[23.06]	[23.05]	[23.04]	[23.04]	[23.03]	[23.03]	

(*continued on next page*)

Table 2 (*continued*)

Mode No.	Crack functions (N_c)	Polynomial solution size ($N_x \times N_y$) at [ ] $N_z = 3$; ( ) $N_z = 4$; { } $N_z = 5$							Stahl and Keer [2]* and Huang et al. [16]+
		3×3	4×4	5×5	6×6	7×7	8×8	9×9	
		(23.01)	(22.98)	(22.97)	(22.96)	(22.95)	(22.95)	(22.95)	
		{23.01}	{22.98}	{22.97}	{22.96}	{22.95}	{22.95}	{22.95}	
	5	[23.07]	[23.04]	[23.04]	[23.03]	[23.03]	[23.03]	[23.03]	
		(22.99)	(22.96)	(22.96)	(22.95)	(22.95)	(22.95)	(22.95)	
		{22.99}	{22.96}	{22.96}	{22.95}	{22.95}	{22.95}	{22.94}	
	6	[23.05]	[23.04]	[23.04]	[23.03]	[23.03]	[23.03]	[23.03]	
		(22.97)	(22.96)	(22.95)	(22.95)	(22.95)	(22.94)	(22.94)	
		{22.97}	{22.95}	{22.95}	{22.95}	{22.95}	{22.94}	{22.94}	
5									27.12*, 25.59+
	0	[38.98]	[38.98]	[38.98]	[29.19]	[29.17]	[28.77]	[28.77]	
		(38.98)	(38.98)	(38.98)	(29.07)	(29.06)	(28.66)	(28.66)	
		{38.98}	{38.98}	{38.98}	{29.07}	{29.06}	{28.66}	{28.66}	
	2	[34.83]	[32.89]	[29.77]	[27.36]	[27.23]	[26.95]	[26.89]	
		(34.65)	(32.70)	(29.64)	(27.24)	(27.11)	(26.83)	(26.77)	
		{34.65}	{32.70}	{29.64}	{27.24}	{27.11}	{26.83}	{26.77}	
	4	[26.07]	[25.98]	[25.85]	[25.85]	[25.82]	[25.81]	[25.80]	
		(25.95)	(25.85)	(25.74)	(25.73)	(25.70)	(25.69)	(25.68)	
		{25.94}	{25.85}	{25.74}	{25.73}	{25.70}	{25.69}	{25.68}	
	5	[25.86]	[25.82]	[25.79]	[25.78]	[25.76]	[25.76]	[25.75]	
		(25.75)	(25.70)	(25.67)	(25.66)	(25.65)	(25.64)	(25.63)	
		{25.75}	{25.70}	{25.67}	{25.66}	{25.65}	{25.64}	{25.63}	
	6	[25.83]	[25.78]	[25.75]	[25.75]	[25.74]	[25.74]	[25.74]	
		(25.71)	(25.66)	(25.64)	(25.64)	(25.63)	(25.63)	(25.62)	
		{25.71}	{25.66}	{25.64}	{25.64}	{25.63}	{25.62}	{25.62}	

When a plate with an internal crack as shown in Fig. 1 is under consideration, there are two crack fronts. The following special functions called crack functions are introduced to express $\widehat{U}_{ic}$ in Eq. (5),

$$\widehat{U}_{ic} = g_i(x,y,z)\sum_{m=1,2}^{N_{iz}}\left\{\sum_{n=1}^{N_{i\_1}}\sum_{l=0}^{n}B_{mnl}^{(i)}r_1^{(2n-1)/2}\cos\frac{2l+1}{2}\theta_1 + \sum_{n=1}^{N_{i\_2}}\sum_{l=0}^{n}\tilde{B}_{mnl}^{(i)}r_2^{(2n-1)/2}\cos\frac{2l+1}{2}\theta_2 + r_2^{\beta}\sin^2(\theta_2/2)\sum_{n=1}^{N_{i\_1}}\sum_{l=0}^{n}C_{mnl}^{(i)}r_1^{(2n-1)/2}\sin\frac{2l+1}{2}\theta_1 + r_1^{\beta}\sin^2(\theta_1/2)\sum_{n=1}^{N_{i\_2}}\sum_{l=0}^{n}\tilde{C}_{mnl}^{(i)}r_2^{(2n-1)/2}\sin\frac{2l+1}{2}\theta_2\right\}z^{m-1} \quad (10)$$

where $g_i(x, y, z)$ ($i = 1, 2, 3$) are included to satisfy the geometric boundary conditions for U_i on the plate faces. The crack functions are expected to work well in the Ritz solution because a similar methodology was applied to study vibrations of a Mindlin plate with an internal crack in [16].

Notably, because $\sin\left(\frac{2l+1}{2}\theta_1\right)$ with $l = 0, 1, 2, \ldots$ in Eq. (10) are discontinuous at $\theta_1 = \pm\pi$, these functions are multiplied by $\sin^2(\theta_2/2)$ to force the resulting functions to be continuous across the plane $\theta_2 = 0$. Moreover, $\sin^2(\theta_2/2)$ is symmetric with respect to $\theta_2 = 0$ and does not change the symmetry of the term $\sin\left(\frac{2l+1}{2}\theta_1\right)$ upon multiplication. Hence, $\sin^2(\theta_2/2)\sin\left(\frac{2l+1}{2}\theta_1\right)$ remains anti-symmetric with respect to the plane of the crack. The singularity at $r_2 = 0$ is found in the first derivatives of $\sin^2(\theta_2/2)$ with respect to x and y; then, $\sin^2(\theta_2/2)$ is multiplied by r_2^{β} with $\beta \geqslant 0.5$ to ensure that incorrect singular behaviors for stresses near $r_2 = 0$ are not obtained. The same applies to the $\sin\left(\frac{2l+1}{2}\theta_2\right)$ terms. In the following analyses, $\beta = 1.5$ is used to ensure that $r_i^{\beta}\sin^2(\theta_i/2)$ ($i = 1$ and 2) yields no stress singularities. Consequently, the admissible functions in Eq. (10) result in the correct stress singularity order at $r_1 = 0$ and $r_2 = 0$.

For simplicity, set $N_{i\_1} = N_{i\_2} = N_c$, $N_{ix} = N_x$, $N_{iy} = N_y$, and $N_{iz} = N_z$ for $i = 1$, 2, and 3 in Eqs. (6) and (10) herein. Substituting Eqs. (6) and (10) into Eqs. (2) and (3) and minimizing the energy functional Π with respect to the to-be-determined coefficients $A_{jkl}^{(i)}, B_{mnl}^{(i)}, C_{mnl}^{(i)}, \tilde{B}_{mnl}^{(i)}$, and $\tilde{C}_{mnl}^{(i)}$ yield $3N_z(N_x \times N_y + 2N_c \times (N_c + 3))$ linear algebraic homogenous equations for those coefficients. An eigenvalue problem is thus obtained, in which the eigenvalues are the natural frequencies of the plate.

A FORTRAN computer program with variables of 128-bit precision was developed. Subroutines "DQDAG" and "DTWODQ" in IMSL were adapted to evaluate the integrals of functions involved in establishing the matrixes in the eigenvalue problem. These subroutines integrate a function by means of a globally adaptive scheme based on Gauss–Kronrod rules [35]. "DTWODQ" was applied to the integration of a function with respect to x and y while "DQDAG" was used for the integration with respect to z. When $\widehat{U}_{ic}$ and their derivatives are involved in the integration, the whole integration domain is divided into six sub-domains in x–y plane as shown in Fig. 3, and the crack is not inside any one of the sub-domains. Consequently, the displacement or slope discontinuities do not occur inside any of these integration sub-domains, and "DTWODQ" can be efficiently executed.

4. Convergence and comparison

The Ritz approach herein yields natural frequencies that converge to exact values from the upper bounds as the number of appropriate admissible functions increases sufficiently. Convergence studies were conducted for square plates with different h/b, $\bar{m}$, and boundary combinations to verify the correctness of the proposed solutions. Two types of boundary conditions on side faces 1–4 (see Fig. 1) are considered-SSSS and CFFF, where S, F and C

Table 3
Comparisons of $\omega(b^2/h\sqrt{\rho/E})$ predicted by various theories for homogeneous SSSS square plates with horizontal central cracks.

d/a	h/b	Mode				
		1	2	3	4	5
0.3	0.01	[5.70]	[14.67]	[14.90]	[23.87]	[27.12]
		(5.701)	(14.65)	(14.89)	(23.81)	(27.09)
		{5.701}	{14.65}	{14.89}	{23.82}	{27.11}
	0.05	[5.70]	[14.67]	[14.90]	[23.87]	[27.12]
		(5.589)	(14.19)	(14.55)	(22.90)	(25.59)
		{5.590}	{14.21}	{14.57}	{22.94}	{25.62}
	0.1	[5.70]	[14.67]	[14.90]	[23.87]	[27.12]
		(5.411)	(13.15)	(13.71)	(20.85)	(23.00)
		{5.421}	{13.22}	{13.76}	{20.97}	{23.13}
	0.2	[5.70]	[14.67]	[14.90]	[23.87]	[27.12]
		(4.933)	(10.69)	(11.48)	(16.40)	(17.83)
		{4.960}	{10.84}	{11.61}	{16.64}	{18.06}
0.5	0.01	[5.70]	[13.02]	[14.74]	[23.52]	[24.86]
		(5.347)	(12.96)	(14.71)	(23.46)	(24.76)
		{5.353}	{12.98}	{14.72}	{23.46}	{24.79}
	0.05	[5.70]	[13.02]	[14.74]	[23.52]	[24.86]
		(5.232)	(12.23)	(14.36)	(22.40)	(23.56)
		{5.238}	{12.28}	{14.37}	{22.44}	{23.60}
	0.1	[5.70]	[13.02]	[14.74]	[23.52]	[24.86]
		(5.060)	(11.02)	(13.50)	(20.22)	(21.33)
		{5.069}	{11.10}	{13.55}	{20.35}	{21.44}
	0.2	[5.70]	[13.02]	[14.74]	[23.52]	[24.86]
		(4.612)	(8.640)	(11.32)	(15.73)	(16.71)
		{4.633}	{8.764}	{11.43}	{15.97}	{16.89}

Note: [ ]:classical thin plate theory [2]; ( ): Mindlin plate theory [16]; { }: present 3-D elasticity-based solution.

Table 4
Convergence of frequency parameters $\omega(b^2/h)\sqrt{\rho_c/E_c}$ for a CFFF FGM ($\bar{m}=5$) square thick plate ($h/b=0.1$) having a vertical central crack with $d/a=0.6$.

Mode No.	Crack functions (N_c)	Polynomial solution size ($N_x \times N_y$) at [ ] $N_z=3$; ( ) $N_z=4$; { } $N_z=5$						
		3×3	4×4	5×5	6×6	7×7	8×8	9×9
1	0	[0.7076]	[0.6987]	[0.6915]	[0.6894]	[0.6878]	[0.6870]	[0.6864]
		(0.7063)	(0.6969)	(0.6900)	(0.6879)	(0.6863)	(0.6855)	(0.6849)
		{0.7062}	{0.6968}	{0.6900}	{0.6878}	{0.6862}	{0.6854}	{0.6848}
	2	[0.6599]	[0.6523]	[0.6460]	[0.6441]	[0.6421]	[0.6411]	[0.6401]
		(0.6565)	(0.6489)	(0.6429)	(0.6411)	(0.6390)	(0.6379)	(0.6369)
		{0.6564}	{0.6488}	{0.6429}	{0.6410}	{0.6389}	{0.6378}	{0.6368}
	3	[0.6356]	[0.6322]	[0.6305]	[0.6294]	[0.6287]	[0.6274]	[0.6271]
		(0.6324)	(0.6291)	(0.6274)	(0.6263)	(0.6256)	(0.6245)	(0.6241)
		{0.6323}	{0.6291}	{0.6273}	{0.6263}	{0.6255}	{0.6244}	{0.6240}
	4	[0.6296]	[0.6279]	[0.6271]	[0.6268]	[0.6261]	[0.6258]	[0.6255]
		(0.6265)	(0.6250)	(0.6241)	(0.6238)	(0.6232)	(0.6229)	(0.6225)
		{0.6264}	{0.6249}	{0.6240}	{0.6237}	{0.6231}	{0.6228}	{0.6225}
	5	[0.6273]	[0.6264]	[0.6260]	[0.6258]	[0.6254]	[0.6253]	[0.6250]
		(0.6244)	(0.6235)	(0.6231)	(0.6229)	(0.6225)	(0.6224)	(0.6221)
		{0.6243}	{0.6234}	{0.6230}	{0.6229}	{0.6224}	{0.6223}	{0.6220}
2	0	[1.719]	[1.646]	[1.639]	[1.620]	[1.618]	[1.612]	[1.611]
		(1.710)	(1.632)	(1.624)	(1.606)	(1.603)	(1.598)	(1.597)
		{1.709}	{1.632}	{1.624}	{1.605}	{1.603}	{1.597}	{1.596}
	2	[1.637]	[1.605]	[1.598]	[1.584]	[1.581]	[1.576]	[1.575]
		(1.620)	(1.586)	(1.579)	(1.565)	(1.562)	(1.558)	(1.556)
		{1.619}	{1.586}	{1.578}	{1.564}	{1.561}	{1.557}	{1.556}
	3	[1.597]	[1.586]	[1.584]	[1.580]	[1.577]	[1.574]	[1.573]
		(1.578)	(1.566)	(1.564)	(1.560)	(1.558)	(1.555)	(1.554)
		{1.578}	{1.566}	{1.564}	{1.560}	{1.557}	{1.555}	{1.554}
	4	[1.584]	[1.580]	[1.577]	[1.574]	[1.573]	[1.572]	[1.571]
		(1.564)	(1.561)	(1.558)	(1.556)	(1.555)	(1.554)	(1.553)
		{1.564}	{1.561}	{1.557}	{1.555}	{1.554}	{1.553}	{1.553}
	5	[1.578]	[1.575]	[1.574]	[1.572]	[1.572]	[1.571]	[1.571]
		(1.559)	(1.556)	(1.555)	(1.554)	(1.554)	(1.553)	(1.553)
		{1.559}	{1.556}	{1.555}	{1.554}	{1.553}	{1.553}	{1.552}
3	0	[4.501]	[4.119]	[4.059]	[4.031]	[4.019]	[4.015]	[4.011]
		(4.500)	(4.080)	(4.016)	(3.992)	(3.981)	(3.976)	(3.972)
		{4.500}	{4.079}	{4.014}	{3.990}	{3.979}	{3.975}	{3.971}
	2	[3.601]	[3.564]	[3.526]	[3.502]	[3.479]	[3.465]	[3.453]
		(3.556)	(3.522)	(3.477)	(3.454)	(3.432)	(3.419)	(3.405)
		{3.555}	{3.521}	{3.476}	{3.453}	{3.430}	{3.417}	{3.403}
	3	[3.331]	[3.302]	[3.267]	[3.242]	[3.236]	[3.227]	[3.224]
		(3.285)	(3.256)	(3.225)	(3.202)	(3.196)	(3.187)	(3.184)
		{3.284}	{3.254}	{3.223}	{3.200}	{3.195}	{3.186}	{3.183}

(*continued on next page*)

Table 4 (*continued*)

Mode No.	Crack functions (N_c)	Polynomial solution size ($N_x \times N_y$) at [ ] $N_z = 3$; ( ) $N_z = 4$; { } $N_z = 5$						
		3×3	4×4	5×5	6×6	7×7	8×8	9×9
	4	[3.234]	[3.221]	[3.214]	[3.211]	[3.207]	[3.205]	[3.203]
		(3.194)	(3.181)	(3.175)	(3.172)	(3.168)	(3.166)	(3.164)
		{3.193}	{3.180}	{3.174}	{3.171}	{3.167}	{3.165}	{3.163}
	5	[3.220]	[3.210]	[3.207]	[3.205]	[3.201]	[3.200]	[3.198]
		(3.181)	(3.172)	(3.168)	(3.167)	(3.163)	(3.162)	(3.161)
		{3.180}	{3.171}	{3.167}	{3.166}	{3.162}	{3.161}	{3.160}
4	0	[5.174]	[4.336]	[4.314]	[4.300]	[4.295]	[4.291]	[4.289]
		(5.137)	(4.336)	(4.314)	(4.300)	(4.295)	(4.291)	(4.289)
		{5.136}	{4.336}	{4.314}	{4.300}	{4.295}	{4.291}	{4.289}
	2	[3.884]	[3.847]	[3.831]	[3.823]	[3.818]	[3.814]	[3.812]
		(3.884)	(3.847)	(3.831)	(3.823)	(3.818)	(3.814)	(3.812)
		{3.884}	{3.847}	{3.830}	{3.823}	{3.817}	{3.814}	{3.812}
	3	[3.847]	[3.831]	[3.822]	[3.816]	[3.814]	[3.811]	[3.810]
		(3.846)	(3.831)	(3.822)	(3.815)	(3.813)	(3.811)	(3.809)
		{3.846}	{3.831}	{3.822}	{3.815}	{3.813}	{3.810}	{3.809}
	4	[3.830]	[3.822]	[3.817]	[3.813]	[3.812]	[3.810]	[3.809]
		(3.829)	(3.821)	(3.817)	(3.813)	(3.811)	(3.809)	(3.808)
		{3.829}	{3.821}	{3.817}	{3.813}	{3.811}	{3.809}	{3.808}
	5	[3.820]	[3.815]	[3.814]	[3.812]	[3.810]	[3.809]	[3.808]
		(3.820)	(3.815)	(3.813)	(3.811)	(3.810)	(3.808)	(3.808)
		{3.820}	{3.814}	{3.813}	{3.811}	{3.810}	{3.808}	{3.807}
5	0	[6.377]	[5.793]	[5.139]	[5.112]	[5.077]	[5.074]	[5.070]
		(6.324)	(5.733)	(5.094)	(5.066)	(5.033)	(5.031)	(5.028)
		{6.322}	{5.731}	{5.093}	{5.064}	{5.032}	{5.030}	{5.026}
	2	[5.091]	[5.038]	[4.881]	[4.872]	[4.849]	[4.846]	[4.840]
		(5.041)	(4.986)	(4.839)	(4.829)	(4.806)	(4.803)	(4.797)
		{5.040}	{4.984}	{4.838}	{4.827}	{4.804}	{4.802}	{4.796}
	3	[4.832]	[4.819]	[4.799]	[4.791]	[4.781]	[4.779]	[4.777]
		(4.790)	(4.776)	(4.757)	(4.749)	(4.739)	(4.738)	(4.736)
		{4.789}	{4.775}	{4.756}	{4.748}	{4.738}	{4.737}	{4.735}
	4	[4.801]	[4.789]	[4.779]	[4.777]	[4.775]	[4.774]	[4.772]
		(4.759)	(4.747)	(4.738)	(4.736)	(4.734)	(4.733)	(4.732)
		{4.758}	{4.746}	{4.737}	{4.735}	{4.733}	{4.732}	{4.730}
	5	[4.789]	[4.781]	[4.774]	[4.773]	[4.772]	[4.771]	[4.771]
		(4.748)	(4.740)	(4.733)	(4.732)	(4.731)	(4.730)	(4.730)
		{4.747}	{4.739}	{4.732}	{4.731}	{4.730}	{4.729}	{4.729}

Table 5
Frequency parameters $\omega(b^2/h)\sqrt{\rho_c/E_c}$ for FGM SSSS square thin plates ($h/b = 0.02$) with horizontal internal cracks ($\alpha = 0°$).

$\bar{m}$	$(x_0/a, y_0/b)$	d/a	Mode				
			1	2	3	4	5
0		0	5.965	14.88	14.88	23.76	29.66
	(0.5, 0.5)	0.1	5.939	14.88	14.88	23.74	29.36
		0.3	5.665	14.58	14.84	23.68	26.71
		0.5	5.318	12.82	14.66	23.28	24.52
	(0.5, 0.75)	0.1	5.951	14.76	14.88	23.76	29.50
		0.3	5.789	13.67	14.85	23.63	27.71
		0.5	5.470	12.39	14.72	21.46	23.01
0.2		0	5.536	13.81	13.81	22.06	27.54
	(0.5, 0.5)	0.1	5.513	13.81	13.81	22.04	27.27
		0.3	5.259	13.53	13.78	21.99	24.80
		0.5	4.937	11.91	13.61	21.62	22.77
	(0.5, 0.75)	0.1	5.524	13.71	13.81	22.06	27.39
		0.3	5.374	12.70	13.79	21.94	25.74
		0.5	5.078	11.50	13.65	19.95	21.37
5		0	3.925	9.787	9.787	15.62	19.49
	(0.5, 0.5)	0.1	3.906	9.785	9.786	15.61	19.27
		0.3	3.725	9.581	9.760	15.56	17.53
		0.5	3.496	8.419	9.638	15.30	16.10
	(0.5, 0.75)	0.1	3.915	9.706	9.785	15.62	19.38
		0.3	3.808	8.984	9.766	15.53	18.19
		0.5	3.597	8.138	9.685	14.06	15.12

denote simply supported, free and clamped, respectively. The geometric boundary conditions of SSSS plates are $U_2 = U_3 = 0$ at $x = 0$ and $x = a$, and $U_1 = U_3 = 0$ at $y = 0$ and $y = b$. Thus, in Eq. (10), $g_1(x, y, z) = y(b - y)$, $g_2(x, y, z) = x(a - x)$, and $g_3(x, y, z) = x(a - x)y(b - y)$. For the CFFF plates, $g_i(x, y, z) = x$ for $i = 1$, 2 and 3 in Eq. (10). In the following, Poisson's ratio is set to 0.3 for homogeneous plates.

Since the literature includes no results concerning vibrations of a plate with an internal crack based on three-dimensional elasticity theory, the published results based on plate theories are used to

Table 6
Frequency parameters $\omega(b^2/h)\sqrt{\rho_c/E_c}$ for FGM SSSS square thick plates ($h/b = 0.2$) with horizontal internal cracks ($\alpha = 0°$).

$\bar{m}$	$(x_0/a, y_0/b)$	d/a	Mode				
			1	2	3	4	5
0		0	5.304	9.742	9.742	11.65	11.65
	(0.5,0.5)	0.1	5.258	9.742	9.742	11.60	11.64
		0.3	4.959	9.728	9.742	10.84	11.60
		0.5	4.633	8.763	9.638	9.742	9.974
	(0.5,0.75)	0.1	5.272	9.714	9.742	11.47	11.64
		0.3	5.059	9.465	9.728	10.55	11.58
		0.5	4.710	8.969	9.483	9.632	10.28
0.2		0	4.950	9.280	9.280	10.92	10.92
	(0.5,0.5)	0.1	4.907	9.280	9.280	10.88	10.92
		0.3	4.627	9.266	9.280	10.18	10.88
		0.5	4.322	8.245	9.183	9.280	9.500
	(0.5,0.75)	0.1	4.920	9.254	9.280	10.75	10.91
		0.3	4.723	9.017	9.267	9.880	10.86
		0.5	4.397	8.544	8.877	9.175	9.795
5		0	3.406	6.296	6.296	7.347	7.347
	(0.5,0.5)	0.1	3.377	6.296	6.296	7.317	7.346
		0.3	3.185	6.274	6.296	6.823	7.322
		0.5	2.976	5.462	6.257	6.296	6.444
	(0.5,0.75)	0.1	3.386	6.278	6.296	7.241	7.341
		0.3	3.247	6.119	6.279	6.656	7.303
		0.5	3.020	5.800	5.883	6.211	6.714

Table 7
Frequency parameters $\omega(b^2/h)\sqrt{\rho_c/E_c}$ for FGM CFFF square moderately thick plates ($h/b = 0.1$) with horizontal or vertical internal cracks.

$\bar{m}$	α	d/a	Mode				
			1	2	3	4	5
0		0	1.042	2.446	6.107	6.601	7.732
	0°	0.1	1.041	2.439	6.103	6.582	7.649
		0.3	1.041	2.419	6.102	6.426	7.198
		0.5	1.039	2.399	6.088	6.117	6.576
	90°	0.1	1.039	2.440	6.056	6.584	7.704
		0.3	1.020	2.420	5.727	6.427	7.567
		0.5	0.9795	2.398	5.185	6.096	7.398
0.2		0	0.9678	2.275	5.682	6.289	7.193
	0°	0.1	0.9675	2.269	5.682	6.273	7.120
		0.3	0.9667	2.251	5.680	6.125	6.703
		0.5	0.9648	2.233	5.665	5.828	6.122
	90°	0.1	0.9651	2.270	5.635	6.273	7.167
		0.3	0.9473	2.251	5.330	6.123	7.039
		0.5	0.9100	2.231	4.826	5.808	6.882
5		0	0.6844	1.595	3.969	4.287	5.026
	0°	0.1	0.6843	1.591	3.969	4.276	4.973
		0.3	0.6837	1.577	3.967	4.175	4.674
		0.5	0.6824	1.562	3.956	3.973	4.262
	90°	0.1	0.6825	1.591	3.935	4.276	5.007
		0.3	0.6694	1.577	3.719	4.174	4.918
		0.5	0.6423	1.561	3.365	3.960	4.808

validate the present solutions. Consequently, Table 2 summarizes the convergence studies of the first five non-dimensional frequency parameters $\omega(b^2/h)\sqrt{\rho/E}$ for a simply supported homogeneous square thin plate ($h/b = 0.05$) having a horizontal central crack ($(x_0/a, y_0/b) = (0.5, 0.5)$) with crack length $d/a = 0.3$. The results were obtained using orthogonal polynomials $N_x \times N_y = 3 \times 3$, $4 \times 4, \ldots, 9 \times 9$, ordinary polynomials $N_z = 3, 4, 5$, and crack functions $N_c = 0, 2, 4, 5, 6$. Table 2 also lists the published non-dimensional frequencies obtained using the classical thin plate theory [2] and Mindlin plate theory [16]. Stahl and Keer [2] used an accurate Fredholm integration approach, while Huang et al. [16] employed the Ritz method with the admissible functions including a set of crack functions that are suitable for the Midlin plate theory with the shear correction factor equal to $\pi^2/12$. Using only polynomials as admissible functions gives incorrect convergent solutions as the number of admissible functions is increased. The incorrect convergent results are the frequencies for an intact plate. Adding crack functions into the admissible functions yields upper bounds that converge to the values that agree excellently with the published results of Huang et al. [16]. As expected, the convergent non-dimensional frequencies are somewhat lower than those of Stahl and Keer [2] that were obtained using the classical thin plate theory, which neglects shear deformation. Using the admissible functions with $N_x \times N_y = 9 \times 9$, $N_z = 4$ and $N_c = 6$ (totally 2268 terms) gives the frequencies that converge to at least three significant figures.

Table 3 compares the first-five non-dimensional frequencies herein with published results obtained using classical plate theory [2] and Mindlin plate theory [16] for SSSS homogeneous cracked square plates with different thickness-to-length ratios. The non-dimensional frequencies in Table 3 are for centrally cracked plates with four different thickness-to-length ratios ($h/b = 0.01$, 0.05, 0.1 and 0.2) and horizontal cracks of two lengths ($d/a = 0.3$ and 0.5). For comparison, only the frequencies for the out-of-plane modes

Table 8
Frequency parameters $\omega(b^2/h)\sqrt{\rho_c/E_c}$ for FGM CFFF square thick plates ($h/b = 0.2$) with horizontal or vertical internal cracks.

$\bar{m}$	α	d/a	Mode				
			1	2	3	4	5
0		0	1.016	2.233	3.306	5.361	6.828
	0°	0.1	1.016	2.227	3.298	5.361	6.750
		0.3	1.016	2.195	3.221	5.359	6.285
		0.5	1.014	2.160	3.065	5.339	5.671
	90°	0.1	1.013	2.227	3.298	5.315	6.805
		0.3	0.9897	2.195	3.220	5.010	6.686
		0.5	0.9431	2.156	3.055	4.529	6.162
0.2		0	0.9448	2.084	3.150	5.012	6.372
	0°	0.1	0.9447	2.077	3.142	5.012	6.300
		0.3	0.9441	2.049	3.069	5.010	5.869
		0.5	0.9426	2.017	2.920	4.990	5.300
	90°	0.1	0.9417	2.078	3.142	4.969	6.350
		0.3	0.9203	2.048	3.068	4.684	6.239
		0.5	0.8774	2.013	2.911	4.233	5.872
5		0	0.6637	1.432	2.154	3.396	4.347
	0°	0.1	0.6637	1.427	2.148	3.396	4.297
		0.3	0.6633	1.406	2.098	3.394	3.992
		0.5	0.6622	1.381	1.998	3.380	3.586
	90°	0.1	0.6615	1.427	2.149	3.367	4.333
		0.3	0.6458	1.405	2.098	3.172	4.259
		0.5	0.6145	1.378	1.991	2.862	4.032

Table 9
Frequency parameters $\omega(b^2/h)\sqrt{\rho_c/E_c}$ for FGM CFCF square thick plates ($h/b = 0.2$) with internal cracks ($\alpha = 90°$ or 150°).

$\bar{m}$	$(x_0/a, y_0/b)$	α	d/a	Mode				
				1	2	3	4	5
0			0	5.382	6.089	8.893	9.536	12.28
	(0.5,0.5)	90°	0.1	5.351	6.089	8.891	9.492	12.26
			0.3	5.148	6.080	8.891	9.263	11.84
			0.5	4.857	6.024	8.873	9.105	9.933
		150°	0.1	5.374	6.089	8.888	9.423	12.28
			0.3	5.325	6.063	8.785	8.881	12.14
			0.5	5.268	5.965	8.105	8.781	10.59
	(0.25,0.5)	90°	0.1	5.374	6.084	8.865	9.513	12.22
			0.3	5.261	6.050	8.605	9.254	11.78
			0.5	4.922	5.984	8.125	8.678	11.22
0.2			0	5.050	5.715	8.473	8.940	11.58
	(0.5,0.5)	90°	0.1	5.020	5.713	8.471	8.897	11.56
			0.3	4.827	5.707	8.470	8.679	11.18
			0.5	4.550	5.654	8.452	8.530	9.374
		150°	0.1	5.041	5.715	8.467	8.834	11.58
			0.3	4.995	5.691	8.237	8.461	11.45
			0.5	4.941	5.600	7.599	8.361	9.988
	(0.25,0.5)	90°	0.1	5.042	5.711	8.446	8.919	11.52
			0.3	4.938	5.679	8.199	8.677	11.10
			0.5	4.623	5.618	7.741	8.135	10.57
5			0	3.400	3.820	5.774	5.976	7.609
	(0.5,0.5)	90°	0.1	3.382	3.820	5.774	5.950	7.598
			0.3	3.259	3.815	5.773	5.813	7.348
			0.5	3.082	3.782	5.715	5.773	6.173
		150°	0.1	3.395	3.820	5.774	5.905	7.607
			0.3	3.365	3.805	5.490	5.752	7.531
			0.5	3.330	3.748	5.035	5.602	6.704
	(0.25,0.5)	90°	0.1	3.395	3.817	5.756	5.962	7.570
			0.3	3.321	3.795	5.591	5.798	7.296
			0.5	3.103	3.751	5.284	5.439	6.949

are given. As expected, the three different theories yield highly consistent vibration frequencies for very thin plates ($h/b = 0.01$). The variation among the results is less than 1%. When the thickness-to-length ratio changes from 0.01 to 0.05, the results obtained using classical plate theory become significantly larger than those obtained using the other theories, and the differences may exceed 6%. The differences become even greater as the thickness-to-length ratio increases. The frequencies obtained using Mindlin plate theory are lower than the three-dimensional results, and their variation is less than 2% even when the thickness-to-length ratio is 0.2.

Table 4 presents the convergence of the non-dimensional frequencies for a moderately thick ($h/b = 0.1$) and cantilevered (CFFF) FGM square plate with a vertical central crack and a crack length of $d/a = 0.6$. The plate is made of aluminum (Al) and alumina (Al_2O_3),

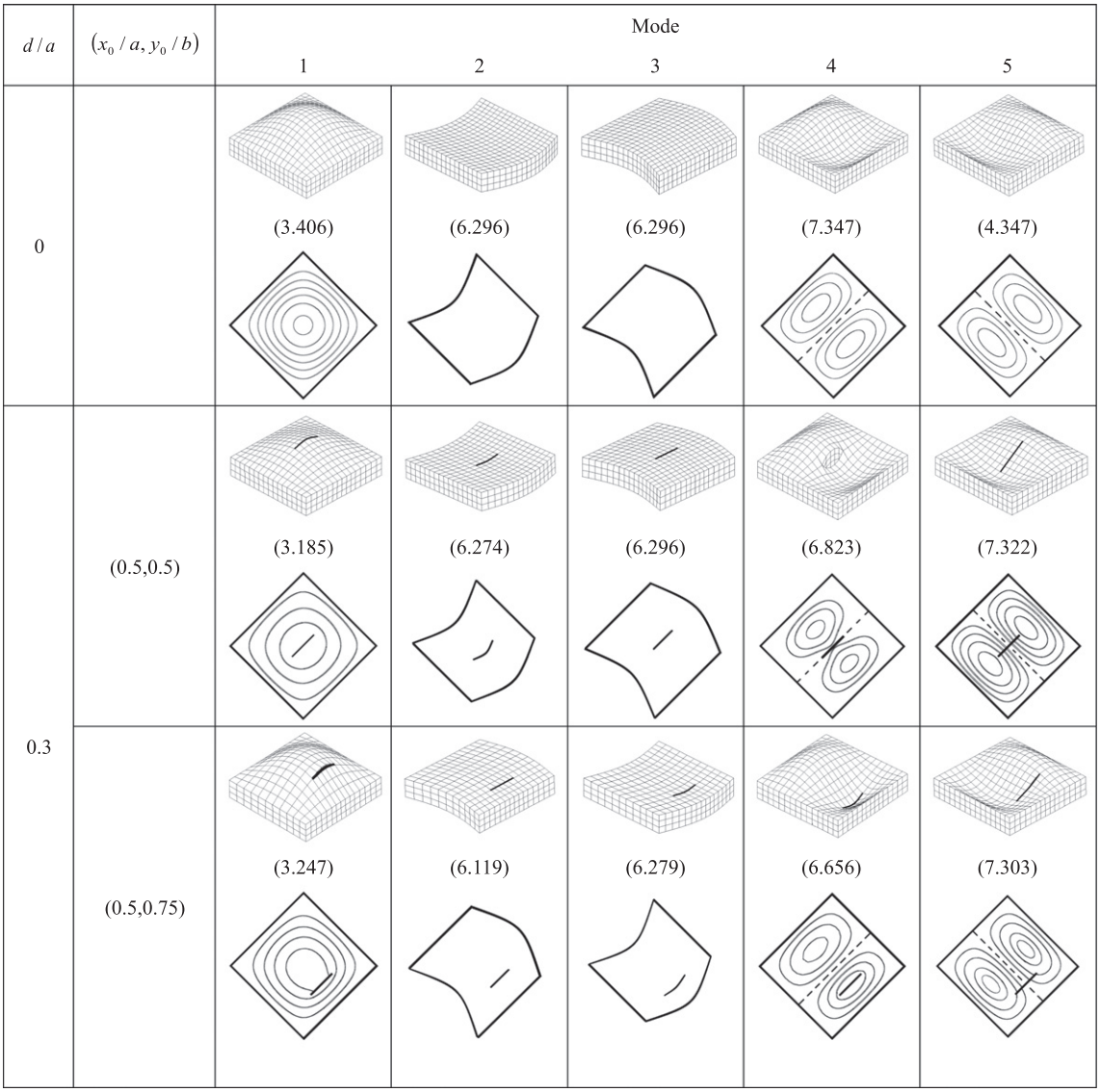

Fig. 4. Mode shapes, nodal patterns and $\omega(b^2/h)\sqrt{\rho_c/E_c}$ for a SSSS square FGM thick cracked plate ($h/b = 0.2$, $\alpha = 0^o$).

and the material properties vary according to Eq. (1) with $\bar{m} = 5$ in the thickness direction. The non-dimensional frequency parameter $\omega(b^2/h)\sqrt{\rho_c/E_c}$, in which subscript "$c$" refers to ceramic ($Al_2O_3$), is adopted. The numerical results were obtained using orthogonal polynomials $N_x \times N_y = 3 \times 3, 4 \times 4, \ldots, 9 \times 9$, ordinary polynomials $N_z = 3, 4, 5$ and crack functions $N_c = 0, 2, 3, 4, 5$. The convergent results that were obtained using no crack functions agree well with those obtained by Zhao et al. [20] using Mindlin plate theory. Zhao et al. [20] employed the element-free kp-Ritz method to obtain the first four non-dimensional frequencies of an intact FGM plate, which are 0.6768, 1.568, 3.927 and 4.263. Incorporating crack functions into the admissible functions substantially enhances the convergence of solutions. Using the admissible functions with $N_x \times N_y = 9 \times 9$, $N_z = 5$ and $N_c = 5$ (a total of 2415 terms) gives the solutions that are accurate to at least three significant figures, while using the admissible functions with $N_x \times N_y = 3 \times 3$, $N_z = 5$ and $N_c = 5$ (a total of 1335 terms) yields results that are accurate to two significant figures.

To further confirm the accuracy of the proposed solutions, the non-dimensional frequencies for the same case as Table 4 except for $\bar{m} = 1$ were determined by the present approach and a finite element method. Using the admissible functions with $N_x \times N_y = 9 \times 9$, $N_z = 5$ and $N_c = 5$ gives the first five non-dimensional frequencies $\omega(b^2/h)\sqrt{\rho_c/E_c}$, which are 0.7494, 1.841, 3.983, 5.072, and 5.669, respectively. The first five non-dimensional frequencies determined by the ABAQUS finite element package, in which twenty-node isoparametric quadratic brick elements (C3D20R) were used, are 0.7493, 1.841, 3.984, 5.092, and 5.670. These results were obtained using 80 elements in each of x and y directions and 128 elements in z direction (resulting in 1,958,184 nodes). Because the material properties linearly vary in z direction, material properties in an element were set equal to the average material properties in the element. An excellent agreement is found between the present results and the finite element results.

5. Frequencies and nodal patterns

Following verification of its convergence and high accuracy, the developed approach is employed to compute the non-dimensional frequency parameters $\omega(b^2/h)\sqrt{\rho_c/E_c}$ for FGM square plates with various thickness-to-length ratios, boundary conditions and internal cracks with various locations, angles of inclination, and lengths. Three classes of boundary conditions on side faces 1–4 (see Fig. 1)

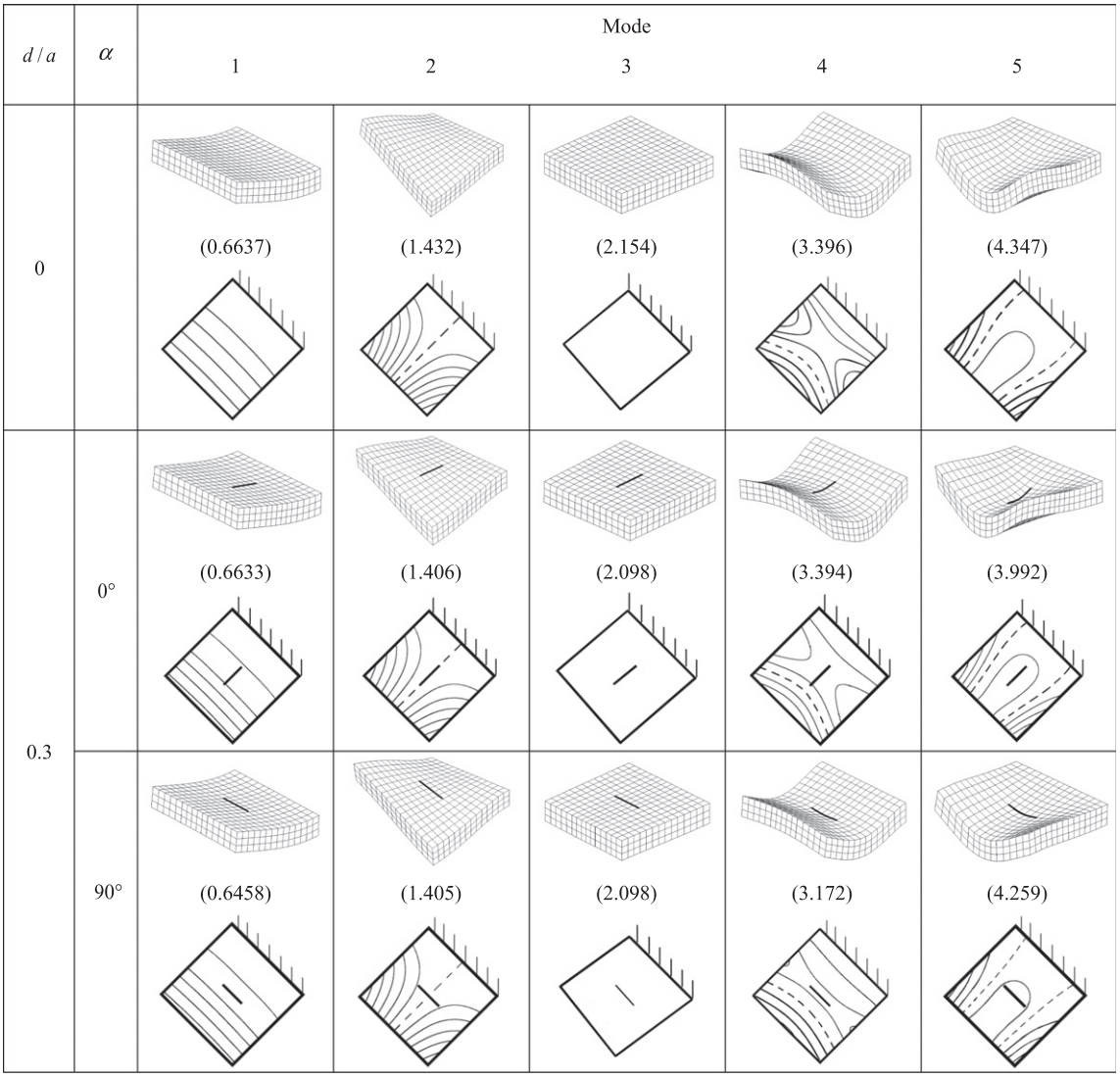

Fig. 5. Mode shapes, nodal patterns and $\omega(b^2/h)\sqrt{\rho_c/E_c}$ for a CFFF square FGM thick plate with a central crack ($h/b = 0.2$, $(x_0/a, y_0/b) = (0.5, 0.5)$).

are considered. They are SSSS, CFFF and CFCF. The frequencies of plates with h/b less than 0.05 and larger than (or equal to) 0.1 were obtained using the admissible functions with $N_z = 4$ and $N_z = 5$, respectively. The admissible functions with $N_x = N_y = 10$ and no crack functions were used for intact plates. The results for cracked plates with crack lengths (d/a) less than 0.3 were obtained using the admissible functions with $N_x = N_y = 8$ and $N_c = 5$; in other cases $N_x = N_y = 9$ and $N_c = 5$ were used. The results given below are exact to at least three significant figures according to the comprehensive convergence studies in the preceding section and extensive convergence studies that are not shown herein. In the following, the plates under consideration are made of aluminum (Al) and alumina (Al_2O_3), and their material properties vary in the thickness direction according to Eq. (1) with $\bar{m} = 0, 0.2$ and 5. The crack length (d/a) are equal to 0, 0.1, 0.3 and 0.5.

Tables 5 and 6 list the first five non-dimensional frequency parameters for SSSS square plates ($h/b = 0.02$ and 0.2) with horizontal central cracks of various lengths at $(x_0/a, y_0/b) = (0.5, 0.5)$. As expected, an increase in the length of the crack reduces the stiffness of the plate and the frequencies. The non-dimensional frequencies also fall as the thickness of the plate increases because the definition of the non-dimensional frequency parameter involves thickness. The frequencies decrease as $\bar{m}$ increases because increasing $\bar{m}$ reduces the stiffness more than it does the mass of the plate. When the location of the crack changes from $(x_0/a, y_0/b) = (0.5, 0.5)$–$(0.5, 0.75)$, the frequencies of the first mode increase, and the frequencies of the other modes may increase or decrease, depending on the mode number and the crack length. A small crack with $d/a = 0.1$ only reduces the first five frequencies of the plate less than 2% relative to those for an intact plate. A large crack with $d/a = 0.5$ reduces the fifth mode frequency of a thin plate ($h/b = 0.02$) and the fourth mode frequency of a thick plate ($h/b = 0.2$) by as much as 22% and 17%, respectively. Tables 7 and 8 display the first five non-dimensional frequencies for CFFF square plates with $h/b = 0.1$ and 0.2, respectively. The two considered angles of inclination of the crack are $\alpha = 0°$ and $\alpha = 90°$. As do those in Tables 5 and 6, the non-dimensional frequencies in Tables 7 and 8 decrease as the thickness of the plate, crack length or value of $\bar{m}$ increases. As the angle of inclination of the crack changes from 0° to 90°, the frequencies of the first mode and the third mode decrease, indicating that the stiffness decreases in these two modes. However, the frequencies of the fifth mode vary oppositely. Again, a small crack with $d/a = 0.1$ reduces the frequencies of the plate by less than 2% from those for an intact plate, whereas a large crack with $d/a = 0.5$ decreases the frequencies by up to 16%. Comparisons of the results for plates with horizontal central cracks in Tables 6

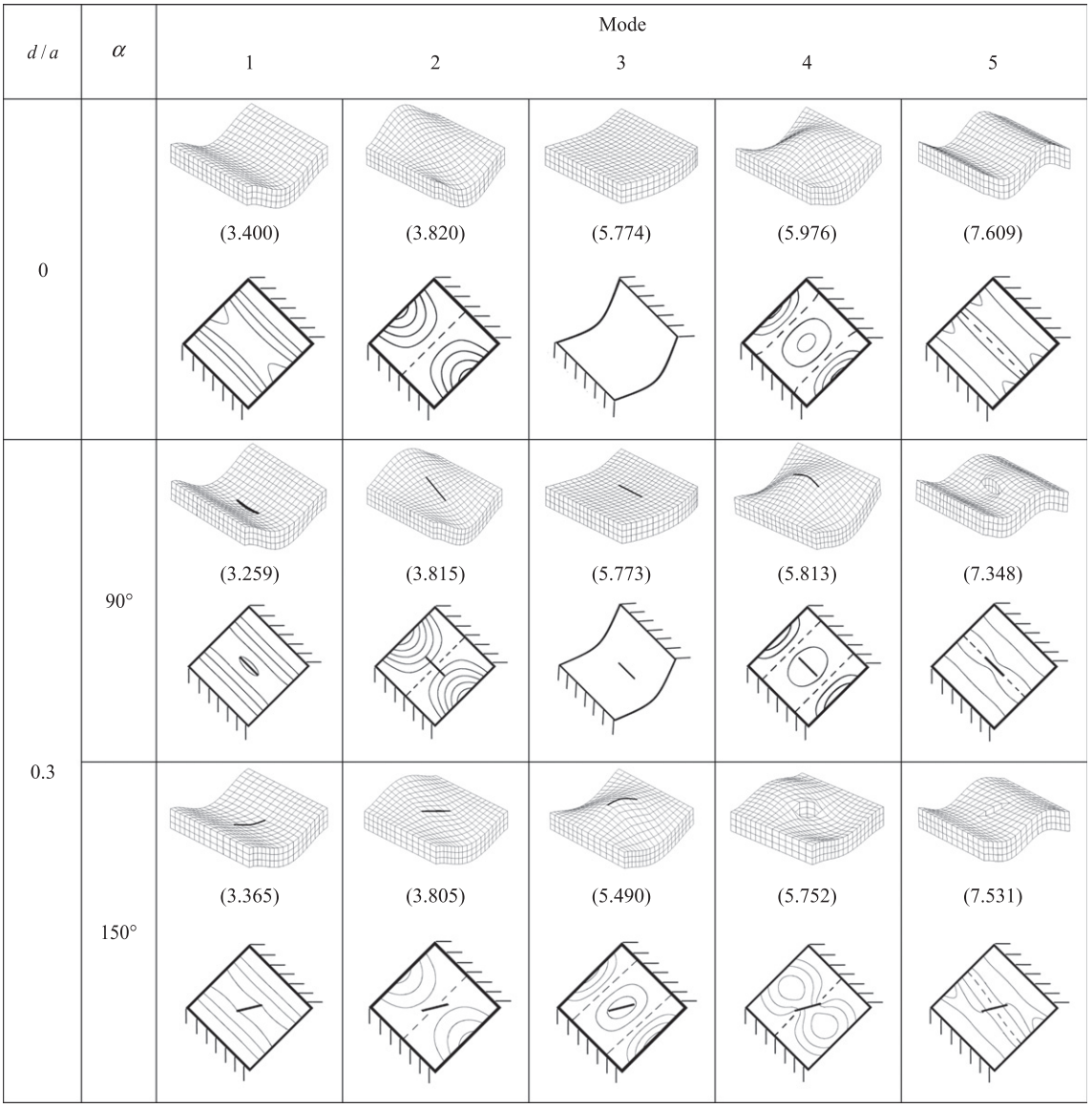

Fig. 6. Mode shapes, nodal patterns and $\omega(b^2/h)\sqrt{\rho_c/E_c}$ for a CFCF square FGM thick plate with a central crack ($h/b = 0.2$, $(x_0/a, y_0/b) = (0.5, 0.5)$).

and 8 reveal that the SSSS plates have higher frequencies than the CFFF plates.

Table 9 summarizes the first five non-dimensional frequencies for CFCF thick square plates ($h/b = 0.2$). Two angles of inclination of the crack are considered – $\alpha = 90°$ and $\alpha = 150°$. As the position of the crack changes from $(x_0/a, y_0/b) = (0.5, 0.5) - (0.25, 0.5)$, the frequencies of the first mode increase while most of the frequencies of the other modes decrease. As the angle of inclination of the crack, α, changes from 90° to 150°, the frequencies of the first and fifth modes increase, and most of the frequencies of the other modes decline. A small crack with $d/a = 0.1$ reduces the frequencies by less than 2% from those of an intact plate, while a large crack with $d/a = 0.5$ reduces the frequencies of the fifth mode by up to 19%. Comparisons of Tables 8 and 9 reveal that CFCF boundary conditions yield higher frequencies than CFFF boundary conditions.

To investigate the effects of a crack on vibration mode shapes, Figs. 4–6 illustrate the first five vibration mode shapes for FGM plates with $h/b = 0.2$, $d/a = 0$ and 0.3, and $\bar{m} = 5$, considered in Tables 6, 8 and 9, respectively. Figs. 4–6 provides three-dimensional vibration mode shapes and the corresponding nodal patterns showing only the deformations on mid-plane. Blank mode shapes indicate in-plane deformation-dominated modes. For the out-of-plane flexural modes, the contour plots for out-of-plane displacement are given, and the nodal lines are represented as dashed lines. Since the value of $\bar{m}$ does not significantly affect the mode shapes, only the results for $\bar{m} = 5$ are depicted. The nodal patterns of the out-of-plane flexural modes for intact SSSS and CFFF plates are very similar to those for homogeneous plates with $h/b = 0.1$ obtained using Mindlin plate theory [16], while the nodal patterns for SSSS and CFFF plates with horizontal central cracks with $d/a = 0.3$ also resemble very much those for cracked homogeneous Mindlin plates with $h/b = 0.1$ and $d/a = 0.2$, presented by Huang et al. [16]. A crack with $d/a = 0.3$ does not make most of the mode shapes for a cracked plate considerably different from those for an intact plate.

6. Concluding remarks

Accurate free vibration analyses of FGM rectangular plates with through internal cracks were carried out using the Ritz method and three-dimensional elasticity theory. New sets of admissible func-

tions, which appropriately describe the stress singularities at the fronts of the crack and displacement discontinuities across the crack, were proposed for displacement fields to supplement sets of polynomials, which can constitute mathematically complete sets of functions. The efficiency of the proposed admissible functions was substantiated through comprehensive convergence studies of non-dimensional frequencies for simply supported, thin homogeneous and cantilevered thick FGM square plates with horizontal central cracks. The convergent results for the cracked thin homogeneous plate ($h/b = 0.05$) agree excellently with previously published results obtained using Mindlin plate theory. Furthermore, an excellent agreement is found between the present results and the results obtained using commercial finite element package ABAQUS for a cracked FGM plate, verifying the correctness and accuracy of the present solutions.

The proposed approach was employed to obtain accurate frequency data for square Al/Al_2O_3 FGM plates with internal cracks. The material properties of FGM are assumed to vary in the thickness direction, in a manner described by a power law. The results are accurate to at least three significant figures. Three types of boundary condition along the four side faces were considered. They were SSSS (simply supported), CFFF (cantilevered) and CFCF. The effects of the volume fraction ($\bar{m} = 0, 0.2$ and 5), thickness-to-length ratio ($h/b = 0.02$, 0.1, 0.2), crack length ($d/a = 0.1$, 0.3 and 0.5), position ($(x_0/a, y_0/b) = (0.5, 0.5)$, $(0.5, 0.75)$ and $(0.25, 0.5)$) and orientation of the crack ($\alpha = 0^\circ$, 90° and 150°) on the non-dimensional frequency parameters $\omega(b^2/h)\sqrt{\rho_c/E_c}$ were investigated. The non-dimensional frequencies decline as thickness-to-length ratio (h/b) or crack length (d/a) increases because the definition of the non-dimensional frequency parameter involves h/b, and the stiffness of the plate decreases with the increase of crack length. The frequencies of the Al/Al_2O_3 FGM plates also decrease as $\bar{m}$ increases. These data can be used as standard to judge the accuracy of other numerical methods and various plate theories.

Acknowledgement

The authors would like to thank the National Science Council of the Republic of China, Taiwan, for financially supporting this research under Contract No. NSC 97-2211-E009-075-MY3.

References

[1] Lynn PP, Kumbasar N. Free vibrations of thin rectangular plates having narrow cracks with simply supported edges. Developments in mechanics, 4, In: Proc 10th midwestern mechanics conference. Fort Collins (CO): Colorado State University; August 21–23, 1967. p. 911–28.
[2] Stahl B, Keer LM. Vibration and stability of cracked rectangular plates. Int J Solids Struct 1972;8(1):69–91.
[3] Aggarwala BD, Ariel PD. Vibration and bending of a cracked plate. Rozprawy Inzynierskie 1981;29(2):295–310.
[4] Neku K. Free vibration of a simply-supported rectangular plate with a straight through-notch. Bull Jpn Soc Mech Eng 1982;25(199):16–23.
[5] Solecki R. Bending vibration of a simply supported rectangular plate with a crack parallel to one edge. Eng Fract Mech 1983;18(6):1111–8.
[6] Hirano Y, Okazaki K. Vibration of cracked rectangular plates. Bull Jpn Soc Mech Eng 1980;23(179):732–40.
[7] Qian GL, Gu SN, Jiang JS. A finite element model of cracked plates and application to vibration problems. Comput Struct 1991;39(5):483–7.
[8] Krawczuk M. Natural vibrations of rectangular plates with a through crack. Arch Appl Mech 1993;63(7):491–504.
[9] Bachene M, Tiberkak R, Rechak S. Vibration analysis of cracked plates using the extended finite element method. Arch Appl Mech 2009;79:249–62.
[10] Yuan J, Dickinson SM. The flexural vibration of rectangular plate systems approached by using artificial springs in the Rayleigh–Ritz method. J Sound Vib 1992;159(1):39–55.
[11] Liew KM, Hung KC, Lim MK. A solution method for analysis of cracked plates under vibration. Eng Fract Mech 1994;48(3):393–404.
[12] Huang CS, Leissa AW. Vibration analysis of rectangular plates with side cracks via the Ritz method. J Sound Vib 2009;323(3–5):974–88.
[13] Huang CS, Leissa AW, Chan CW. Vibrations of rectangular plates with internal cracks or slits. Int J Mech Sci 2011;53:436–45.
[14] Ma CC, Huang CH. Experimental and numerical analysis of vibrating cracked plates at resonant frequencies. Exp Mech 2001;41(1):8–18.
[15] Lee HP, Lim SP. Vibration of cracked rectangular plates including transverse shear deformation and rotary inertia. Comput Struct 1993;49(4):715–8.
[16] Huang CS, Leissa AW, Li RS. Accurate vibration analysis of thick, cracked rectangular plates. J Sound Vib 2011;330:2079–93.
[17] Abrate S. Functionally graded plates behave like homogeneous plates. Compos B Eng 2008;39:151–8.
[18] Zhang DG, Zhou YH. A theoretical analysis of FGM thin plates based on physical neutral surface. Comput Mater Sci 2008;44(2):716–20.
[19] Hosseini-Hashemi Sh, Rokni Damavandi Taher H, Akhava H, Omidi M. Free vibration of functionally graded rectangular plates using first-order shear deformation plate theory. Appl Math Model 2010;34:3991–4011.
[20] Zhao X, Lee YY, Liew KM. Free vibration analysis of functionally graded plates using the element-free kp-Ritz method. J Sound Vib 2009;319:918–39.
[21] Ferreira AJM, Batra RC, Roque CMC, Qian LF, Jorge RMN. Natural frequencies of functionally graded plates by a meshless method. Compos Struct 2006;75:593–600.
[22] Qian LF, Batra RC, Chen LM. Static and dynamic deformations of thick functionally graded elastic plate by using higher-order shear and normal deformable plate theory and meshless local Petrov–Galerkin method. Compos B Eng 2004;35:685–97.
[23] Roque CMC, Ferreira AJM, Jorge RMN. A radial basis function approach for the free vibration analysis of functionally graded plates using a refined theory. J Sound Vib 2007;300:1048–70.
[24] Matsunaga H. Free vibration and stability of functionally graded plates according to a 2-D higher-order deformation theory. Compos Struct 2008;82:499–512.
[25] Vel SS, Batra RC. Three-dimensional exact solution for the vibration of functionally graded rectangular plates. J Sound Vib 2004;272:703–30.
[26] Reddy JN, Cheng ZQ. Frequency of functionally graded plates with three-dimensional asymptotic approach. J Eng Mech ASCE 2003;129:896–900.
[27] Uymaz B, Aydogdu M. Three-dimensional vibration analysis of functionally graded plates under various boundary conditions. J Reinf Plast Compos 2007;26(18):1847–63.
[28] Huang CS, McGee III OG, Chang MJ. Vibrations of cracked rectangular FGM thick plates. Compos Struct 2011;93:1747–64.
[29] Bhat RB. Natural frequencies of rectangular plates using characteristic orthogonal polynomials in Rayleigh–Ritz method. J Sound Vib 1985;102(4):493–9.
[30] Hartranft RJ, Sih GC. The use of eigenfunction expansions in the general solution of three-dimensional crack problems. J Math Mech 1969;19(2):123–38.
[31] Chaudhuri RA, Xie M. A novel eigenfunction expansion solution for three-dimensional crack problems. Compos Sci Technol 2000;60:2565–80.
[32] Huang CS, Chang MJ. Corner stress singularities in a FGM thin plate. Int J Solids Struct 2007;44(9):2802–19.
[33] Huang CS, Chang MJ. Geometrically induced stress singularities of a thick FGM plate based on the third-order shear deformation theory. Mech Adv Mater Struct 2009;16(2):83–97.
[34] Wang KP. Three-dimensional vibrations of functionally graded material rectangular cracked plates with side cracks. MS thesis, Taiwan: National Chiao Tung University; 2010.
[35] Piessens R, deDoncker-Kapenga E, Uberhuber CW, Kahaner DK. QUADPACK. New York: Springer-Verlag; 1983.